Nuclear Engineering and Design 446 (2026) 114561

Contents lists available at ScienceDirect

Nuclear Engineering and Design

journal homepage: www.elsevier.com/locate/nucengdes

An integrated open-source CFD workflow for gas distribution and flame propagation analysis in nuclear reactor safety

Dario Živković [a,*], Stephan Kelm [b], Thomas Sattelmayer [a]

[a] Chair of Thermodynamics, Technical University of Munich (TUM), Boltzmannstr. 15, Garching, Germany
[b] Institute of Energy Technologies (IET), Forschungszentrum Jülich GmbH, Wilhelm-Johnen-Straße 52428 Jülich, Germany

ARTICLE INFO

Keywords:
Nuclear reactor accident analysis
Lumped parameter (LP) analysis
Computational fluid dynamics (CFD)
Gas mixture formation
Flame propagation

ABSTRACT

A coupled numerical simulation workflow for comprehensive end-to-end analysis of nuclear reactor accidents is introduced with the emphasis on two distinct, open-source Computational Fluid Dynamics (CFD) codes developed within the OpenFOAM framework: *containmentFOAM* for detailed simulation of pre-ignition gas distribution and thermal-hydraulics, and *explosionDynamicsFOAM* for the subsequent flame propagation analysis. A Small Break Loss-of-Coolant Accident (SB–LOCA) scenario in a generic Pressurized Water Reactor (PWR) containment is analyzed, providing critical insights into containment safety, quantifying pre-ignition turbulence, pressure evolution, maximum flame speed, and resolving local flow phenomena such as inter-compartmental gas flows and multiple emerging flame paths. A key improvement of accident analysis in the present work is in the use of a full-scale CFD simulation for obtaining the spatially-resolved turbulence kinetic energy field prior to ignition. This allowed choosing the appropriate combustion modeling approach in the subsequent flame propagation simulation. For the specific SB–LOCA scenario investigated here, the simulations indicated that the flame propagation remained within the deflagration regime, i.e. the flame speeds necessary for a Deflagration-to-Detonation Transition (DDT) were not achieved within the containment volume.

1. Introduction

Gas explosions remain a critical concern in nuclear safety since severe reactor accidents may produce mixtures containing flammable gases such as hydrogen and carbon monoxide. In conditions of a severe accident, a wide range of phenomena can influence the thermal hydraulics and flame propagation behavior within the containment of a water-cooled nuclear reactor. These include turbulence, buoyancy, thermal radiation, convection, fluid–solid interaction, multiphase flow (e.g., water spray), steam condensation and combustion chemistry (Bentaïb et al., 2015; Liu et al., 2021). Additionally, due to practical difficulties and unfeasibility of conducting experiments at plant scales, there is a high demand for the development of suitable numerical simulation methods (Fiorina et al., 2022).

Both general-purpose and tailor-made CFD codes have been applied to nuclear accident analysis with the aim of spatially and temporally resolving the safety-relevant phenomena. Notable examples of tailor-made tools include the GASFLOW suite, comprised of GASFLOW for gas distribution, COM3D for deflagrations, and DET3D for detonations (Travis et al., 1998; Breitung and Royl, 2000), and its successor GASFLOW-MPI (Xiao et al., 2017a). These have been extensively used for analyzing gas dispersion and combustion phenomena in containments of both Pressurized Water Reactor (PWR) and Boiling Water Reactor (BWR) types under diverse accident scenarios such as SB–LOCA and SBO (Breitung et al., 2000; Dimmelmeier et al., 2012; Xiao et al., 2017a; Kang et al., 2020, 2022; Yabing et al., 2022). Other significant efforts in the field include the application of codes such as REACFLOW, developed at the European Commission's Joint Research Centre (JRC) (Wilkening and Huld, 1999; Baraldi et al., 2007), commercial software like CFX (Baraldi et al., 2007) and modifications of the open-source CFD code OpenFOAM, occasionally coupled with initial conditions derived from other simulation tools (Kim and Hong, 2015; Hasslberger et al., 2017a,b). The cited work demonstrated the value of CFD, particularly when simulations are performed at the full containment scale, which allows for capturing large-scale effects crucial for reactor safety analysis.

Simulating combustion events in reactor accident analysis requires realistic initial conditions, such as gas composition, thermodynamic state, and turbulence levels, immediately preceding ignition. While Lumped Parameter (LP) codes very efficiently simulate an accident at a system level, they lack the spatial resolution required to resolve

* Corresponding author.
E-mail address: dario.zivkovic@tum.de (D. Živković).

https://doi.org/10.1016/j.nucengdes.2025.114561
Received 18 May 2025; Received in revised form 4 September 2025; Accepted 20 October 2025
Available online 10 November 2025
0029-5493/© 2025 The Authors. Published by Elsevier B.V. This is an open access article under the CC BY license (http://creativecommons.org/licenses/by/4.0/).

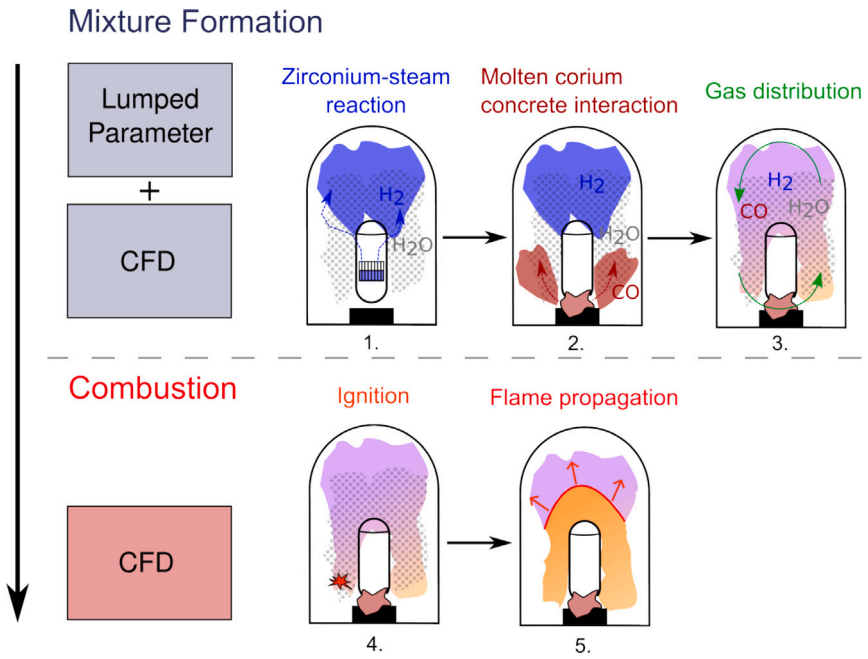

Fig. 1. Overview of the reactor accident analysis workflow: the LP code COCOSYS is first used for the prediction of early accident stages and mixture generation, followed by the CFD analysis of gas mixing with *containmentFOAM*. Subsequently, the flame propagation CFD analysis is performed using *explosionDynamicsFOAM*.

local gas distributions and cannot predict turbulence intensity. Consequently, mapping procedures and assumptions become necessary when utilizing LP results for CFD initialization (Hasslberger et al., 2017b). Alternatively, the assumption of hypothetical scenarios, such as *equivalent stoichiometric flammable clouds* (Daudey and Champassith, 2014) or heuristically prescribed mixture and turbulence intensity fields are employed (Hasslberger et al., 2017a,b). However, such approaches highly depend on the modeling assumptions made and a careful balance between realism and conservatism is needed (Daudey and Champassith, 2014).

The present study emphasizes the necessity for realistic initial conditions obtained through detailed modeling of the gas distribution phase. In contrast to previous studies, which often imposed an assumed turbulence intensity or relied solely on LP code output, *containmentFOAM* (Kelm et al., 2021a) is leveraged here to simulate the buoyancy-driven flow dominating the mixing process prior to ignition. The solution fields from *containmentFOAM* are then used to initialize the combustion simulation with *explosionDynamicsFOAM*. Detailed spatial distributions of gas fractions, temperature and, crucially, a quantitative assessment of the turbulence intensity within the containment atmosphere were produced by this approach. While prior CFD studies on combustion in the context of nuclear accidents universally applied turbulent combustion models (e.g., EBU, EDC, PaSR, TFC), implicitly assuming a turbulent flame regime (Baraldi et al., 2007; Hasslberger et al., 2017a,b; Kim and Hong, 2015), a quantitative assessment of the pre-ignition turbulence field has, to the best of the authors' knowledge, not yet been presented in a full-scale CFD study of a combustion event in a nuclear reactor containment. Furthermore, the modeling framework within *explosionDynamicsFOAM* makes no a priori assumptions of a turbulent flame regime. Based on local conditions, it can adaptively apply either a model for instability-driven flame wrinkling or a turbulent scaling law.

Another objective of this study is to showcase the coupled LP–CFD workflow (Fig. 1). The solution from Containment Code System (COCOSYS), an LP code, regarding the initial accident stages was used as a starting point. Subsequently, CFD analyses were performed using two tailor-made OpenFOAM-based solvers: *containmentFOAM* for detailed gas distribution and thermal-hydraulic analysis and *explosionDynamicsFOAM* for the following flame propagation simulation. Both CFD

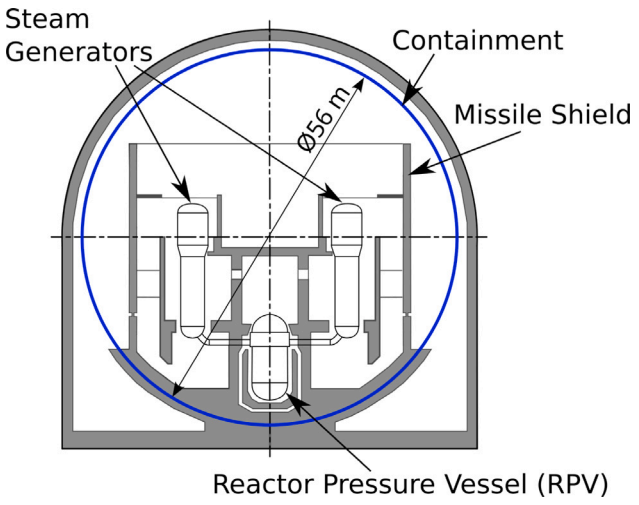

Fig. 2. The *Konvoi*-type reactor containment.

simulations included the full geometric scale of the *Generic Containment* (Kelm et al., 2014), a standardized benchmark model derived from the *Konvoi* PWR containment shown in Fig. 2. Ultimately, the results of the combustion simulation provide the peak pressure and flame speeds reached under the analyzed accident conditions.

2. Numerical methods

2.1. Gas distribution simulation (containmentFOAM)

The simulation of the gas distribution and mixing phase within the containment prior to ignition was performed using the specialized OpenFOAM-based CFD solver *containmentFOAM* (Kumar et al., 2019; Kelm et al., 2021a). It was explicitly developed to analyze the complex thermal-hydraulic phenomena occurring during nuclear reactor accidents, such as multi-species gas transport, aerosol/particle dynamics, turbulent flow, and conjugate and radiative heat transfer. The

capabilities of *containmentFOAM* in representing relevant reactor accident thermal-hydraulic conditions have been validated against various benchmark cases (Kelm et al., 2019; Kampili et al., 2021). In addition to the reactor safety analysis, *containmentFOAM* has been validated more broadly for applications in hydrogen safety (Yassin et al., 2023) and later applied to an accidental leakage scenario of liquid hydrogen in an industrial building (Yassin et al., 2025).

The development of *containmentFOAM* was based on the open-source CFD code OpenFOAM (Weller et al., 1998), which solves the discretized integral form of the governing Navier–Stokes equations using the cell-centered Finite Volume Method (FVM). The OpenFOAM basic functionality for multicomponent gas modeling was refined by adding enthalpy transport due to inter-species diffusion and accounting for varying specific enthalpies of individual species (Kumar et al., 2019). Furthermore, the solution method was improved by introducing an additional density corrector step in the segregated pressure-based PIMPLE algorithm—a hybrid of PISO (Pressure-Implicit with Splitting of Operators) and SIMPLE (Semi-Implicit Method for Pressure-Linked Equations) (Kumar et al., 2019).

The ongoing work regarding the *containmentFOAM* library is focused on developing required models for containment thermal-hydraulics and related phenomena, e.g., near-wall steam condensation (Vijaya Kumar et al., 2021), efficient modeling of radiative heat transfer (Liu et al., 2022) or Lagrangian-Eulerian modeling of fission-product aerosol transport (Kampili et al., 2018). Moreover, *containmentFOAM* implements a range of system models that are bespoke to the context of reactor accident analysis and represent various installed equipment in the containment, including boundary conditions for conditionally open/closed burst discs and doors, coupling frameworks for Passive Autocatalytic Recombiner (PAR) operation (e.g., with REKODIREKT) and porous media models for plant components under-resolved by the CFD grid (e.g., various metal structures or pipe bundles).

Gas mixtures in *containmentFOAM* are assumed to be composed of ideal gases where Wilke's mixing rule is used for deriving the mixture's transport properties using VDI heat atlas (2013) data, while temperature-dependent heat capacities are provided both by NIST Chemistry Webbook (Lemmon, 2010) and the VDI heat atlas (2013). Multicomponent diffusion is handled by the effective binary diffusion model where pressure- and temperature-dependent binary diffusion coefficients of individual species are calculated according to Fuller et al. (1966).

In turbulence modeling for buoyancy-driven flows, it is key to consider the production and dissipation of turbulence due to the effect of buoyancy force, which is neglected in general-purpose turbulence models for CFD (Kelm et al., 2021a). In *containmentFOAM*, the k-ω Shear Stress Transport (SST) model is corrected for the buoyancy production term in the turbulent kinetic energy equation using the Simple Gradient Diffusion Hypothesis (SGDH) (Chung and Devaud, 2008).

In the present work, the radiative heat transfer was modeled using the P1 radiation model (Howell et al., 2020) with constant absorption coefficients prescribed for gas mixture components, with the participating gases in the present work being H_2O and CO.

2.2. Flame propagation simulation (explosionDynamicsFOAM)

The flame propagation analysis was performed using *explosionDynamicsFOAM*, a custom solver based on the OpenFOAM CFD library (Weller et al., 1998). The *explosionDynamicsFOAM* solver is a density-based, unstructured, second-order FVM simulation tool designed to solve the unsteady, compressible, reacting Unsteady Reynolds-averaged Navier–Stokes (URANS) equations. The coupled set of Navier–Stokes equations includes the terms accounting for the effect of gravitational acceleration on momentum and energy conservation.

The numerical method in *explosionDynamicsFOAM* was designed to capture the continuous flame propagation from ignition to potential Deflagration-to-detonation Transition (DDT) in a single density-based solver framework without requiring a heuristic-dependent solver swapping. This was achieved primarily using *all-speed* convective flux schemes for spatial discretization and a low-storage second-order, Strong Stability Preserving (SSP) Runge–Kutta scheme by Ketcheson (2010) for temporal integration. The SSP Runge–Kutta method was shown to enable greater computational stability and efficiency, particularly in the analysis of reacting flows where simulations using conventional methods typically required a significant reduction in the Courant–Friedrich–Lewy (CFL) condition to achieve numerical stability (Zivkovic and Sattelmayer, 2021).

The working fluid is treated as a thermally perfect gas in *explosionDynamicsFOAM*. Temperature-dependent specific heat capacities are obtained from the NIST-JANAF thermochemical tables (Chase, 1998). The pressure–density relationship is determined by the ideal gas equation of state. The dynamic viscosity μ and its dependence on temperature are described by the empirically derived Sutherland correlation (Sutherland, 1893).

The reacting flow in the deflagration regime is modeled using a transport equation for the reaction progress variable, defined as $b = 1$ in the unburned mixture and $b = 0$ in the burned mixture (Weller et al., 1998b). The statistical interpretation of the progress variable within the Reynolds-averaged Navier–Stokes (RANS) framework was given by Bray and Moss (1977) as well as Bray and Libby (1986). The source term in the progress variable equation, representing the burning rate, is modeled via the gradient closure method (Lipatnikov, 2012; Poinsot and Veynante, 2005). In this formulation, the effective burning rate is the product of the gradient of the progress variable b and the effective flame speed, $S_{\mathrm{eff}} = \Xi S_{\mathrm{l}}$. The laminar flame speed, S_{l}, is determined in the present work using the chemical reaction mechanism of Li et al. (2015), with appropriate corrections for the thermodynamic state and steam dilution.

The flame wrinkling coefficient, Ξ, accounts for the increase in flame surface area due to flame instabilities or turbulence. Its modeling is necessary in large-scale CFD studies and depends on the dominant wrinkling mechanism. In nearly quiescent (or quasi-laminar) conditions, often encountered in industrial-scale safety analyses, flame wrinkling is primarily driven by intrinsic flame instabilities. For these conditions, the deflagration model developed by Zivkovic and Sattelmayer (2023) is used. This model was derived specifically for the effects of the Darrieus–Landau (DL) instability on large-scale flames under low turbulence conditions. It incorporates correction factors for small-scale Thermal–difussive (TD) instability, pressure effects (Katzy et al., 2017a), and flame curvature effects (Katzy, 2021). Although the curvature correction factor was derived initially for pure hydrogen fuel, it was applied in the present study without modification due to a lack of equivalent experimental data for hydrogen–carbon-monoxide mixtures and the relatively low CO concentration in the considered accident scenario, as shown in Fig. 5. In scenarios where turbulence is the dominant wrinkling mechanism, *explosionDynamicsFOAM* can employ various established turbulent scaling laws. Models such as those by Dinkelacker et al. (2011) and Goulier et al. (2017), which have been validated for safety-related combustion analyses, are available within the solver. The transition between instability-driven and turbulence-driven wrinkling models is handled automatically within *explosionDynamicsFOAM*. This selection is based on a chosen criterion, which can be a theoretically-derived condition by either (Chaudhuri et al., 2011) or (Chomiak and Lipatnikov, 2023); or a conservative approach that applies the maximum wrinkling predicted by the two distinct models, i.e., $\max\left(\Xi_{\mathrm{inst.}}, \Xi_{\mathrm{turb.}}\right)$.

The URANS modeling approach is employed to capture the turbulence generated during the flame propagation, which has a potential to significantly influence the flame speed. Specifically, the k-ω SST-Scale Adaptive Simulation (SAS) model by Menter and Egorov (2010) is applied.

Radiative heat transfer was not considered during the flame propagation phase. This simplification is made due to the relatively short duration of this phase (on the order of several seconds), over which radiation effects are assumed to have a less dominant impact on the overall flame dynamics compared to other phenomena.

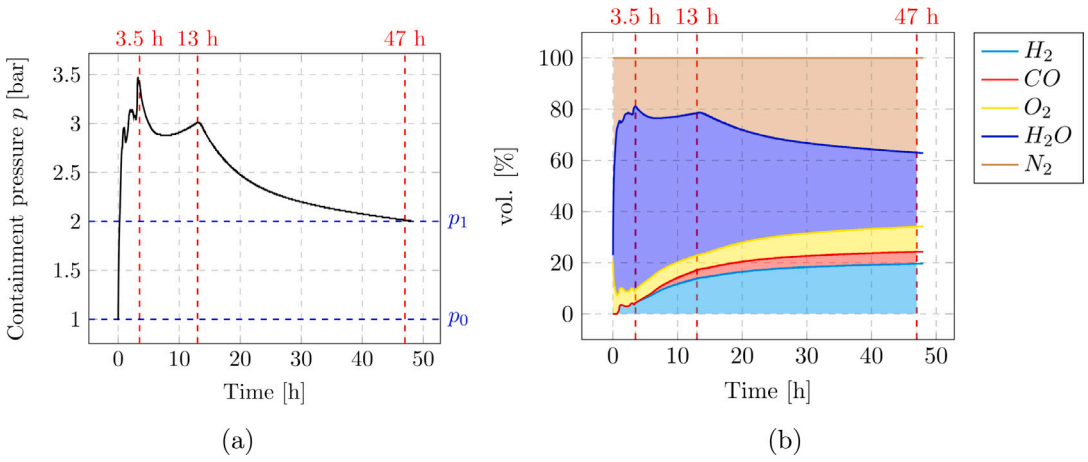

Fig. 3. Development of the containment pressure and mixture composition in the Dome compartment. The red lines indicate key phases of the accident (Table 1). The blue lines indicate p_0 – containment pressure prior to accident, and p_1 – containment pressure at $t = 47\,\text{h}$. The ignition occurs shortly after $t = 47\,\text{h}$.

Table 1
The pre-ignition SB–LOCA accident phases.

Time [h]	Accident phase
0:00	Loss of coolant caused by the failure of one connection of the accumulators.
0:41	The beginning of core melting.
3:06	Lower plenum melt relocation.
03:24	Failure of the RPV and the beginning of MCCI.
13:00	MCCI stabilization in the dry cavity (no further steam releases).
47:00	The mixture ignites at a hot surface (RR compartment).

3. "Generic Containment" Lumped Parameter model of an SB–LOCA accident

The progression of the modeled Small Break – Loss of Coolant (SB–LOCA) accident scenario begins with a break ($50\,\text{cm}^2$ in cross section) in one connection line of the accumulators and thus a loss of primary coolant, leading sequentially to core overheating and the onset of melting. Following the continuous core degradation, the molten corium relocates to the lower plenum of the Reactor Pressure Vessel (RPV). Thereafter, the melt relocates to the reactor cavity beneath once the RPV failure is reached. During the *in-vessel* phase (up to $t = 3.5\,\text{h}$), the containment is primarily pressurized by the released steam and hydrogen (Fig. 3).

The following *ex-vessel* phase is characterized by the Molten Corium Concrete Interaction (MCCI), which generates additional hydrogen (H_2), carbon monoxide (CO) and steam (H_2O) by the decomposition of concrete. In the present work, the dry cavity MCCI stabilization is assumed (Table 1). Although it can be realistically expected that the MCCI penetrates the biological shield and reaches the sump water, which would then quench the melt pool and cause a strong release of steam – resulting in further inertization of the containment atmosphere – the MCCI stabilization scenario was chosen to establish highly reactive mixture conditions conducive to the subsequent flame propagation study. Additionally, PAR operation was conservatively not considered, so that no H_2O, CO, or O_2 were consumed before ignition. Following the assumed MCCI stabilization, the primary phenomenon determining the containment atmosphere remained the condensation of steam due to heat transfer to the environment, which gradually increased the relative concentration of flammable gases. The steam condensation in the present scenario continued until $t = 47\,\text{h}$.

The LP modeling of the SB–LOCA accident scenario detailed here, performed with COCOSYS, corresponds to the modeling benchmark exercises defined in the European research project SAMHYCO-NET, which expanded upon the previously developed standardized *Generic Containment* LP model based on a *Konvoi* PWR type of nominal 1300 MWe (Kelm et al., 2014). The *Generic Containment* benchmark series was comprised of modeling exercises of multiple scenarios with increasing complexity, including varying heat and gas sources.

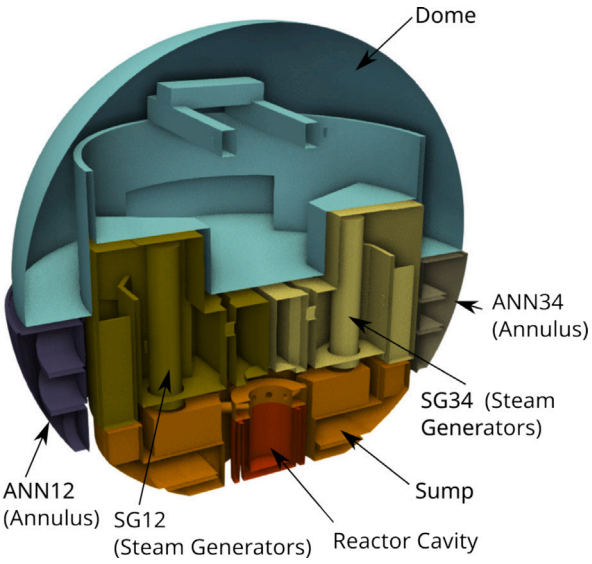

Fig. 4. "Generic Containment" LP zones relevant for gas distribution and flame propagation in the present work.

The design pressure of the *Konvoi* reactor containment is 8 bar, while its total volume of $V \approx 70\,000\,\text{m}^3$ fully encloses the reactor system. The *Generic Containment* LP nodalization simplifies the complex reactor building geometry into 16 interconnected volumes (zones) representing major compartments. The zones are linked via atmospheric (gas) and drain (liquid) junctions, with simplified models for rupture discs and relief flaps with varying opening pressures. At the same time, the heat capacity and surface area were kept equal to the more detailed

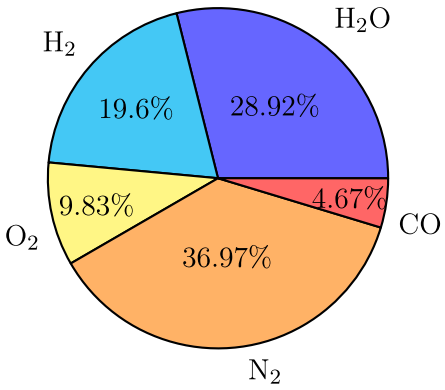

Fig. 5. The gas composition in the containment shortly prior to ignition (t = 47 h from the beginning of the accident).

model developed by Bönigke et al. (1998). Fig. 4 shows the 7 out of 16 LP zones in the *Generic Containment* model that are the most relevant to the present work. The more in-depth presentation of the LP nodalization, together with a detailed schematic of the LP zones and their interconnections can be found in Kelm et al. (2014).

The initial conditions of the LP zones in the COCOSYS simulation consisted of humid air (21 vol.% O2, 79 vol.% N2) with the pre-accident pressure p_0 = 1 bar. The initial temperature of T_0 = 30 °C, and relative humidity of ψ_0 = 50% were present in all containment zones except the reactor cavity, which was at $T_{0,C}$ = 80 °C with $\psi_{0,C}$ = 30% humidity. The zones were assumed to have initially been in thermal equilibrium.

The evolution of containment pressure and gas composition calculated by the LP model is shown in Fig. 3. The pressure result shown in Fig. 3(a) is representative for the containment as a whole, while the mixture composition evolution in the Dome zone in Fig. 3(b) is representative for the inner containment (Dome and SG compartments), which is the most relevant part for the subsequent flame propagation analysis. The peak pressure of just under 3.5 bar was reached at approx. 3.5 h, which dropped after the RPV failure, only to rise again during the MCCI phase to its smaller, secondary peak of 3 bar at t = 13 h. The pressure curve follows closely the steam volume concentration (Fig. 3(b)). After MCCI stabilization at t = 13 h there were no further steam releases and the containment undergoes a slow depressurization due to heat loss toward the environment, as well as steam condensation. The hydrogen production rises sharply in the initial phases of the accident and then later slowly during the MCCI, when carbon monoxide is also produced. The initial oxygen mass remains unchanged due to no PAR operation in the present scenario. The containment pressure at the end of the LP simulation (t = 47 h) reached p_1 = 200 390 Pa (≈ 2 bar).

4. Computational setup of the CFD simulations

The computational domain in this study included the complete internal volume of the *Konvoi* reactor containment. The computational domain for the gas distribution simulation with *containmentFOAM* contained a solid domain for the concrete structures and a fluid domain for the gas mixture (Fig. 7). Given the time scale of the gas mixing simulation measured in minutes, the temperature changes in the solid were considered significant, along with the changes in gas temperature. In the present scenario which assumed MCCI stabilization in the dry cavity, the reactor cavity was not included in the computational domain (Fig. 6(a)).

A temperature mapping on the fluid-solid interface was required in the gas distribution CFD simulation in which the wall temperatures were mapped from the LP zones and kept constant for the duration of the *containmentFOAM* simulation. Furthermore, the wall condensation model by Vijaya Kumar et al. (2021) was applied.

In the case of the flame propagation simulation using *explosionDynamicsFOAM*, only the fluid region was modeled (Fig. 8), given that the combustion process lasted no more than several seconds, during which the change in temperature of the concrete is considered of negligible influence on the overall combustion process. All boundary conditions were set to adiabatic, no-slip walls with *wall functions* applied to turbulent quantities.

The computational grid for the gas distribution simulation with *containmentFOAM* included predominantly hexahedral cells, of which approx. 3.5M were used for discretizing the fluid subdomain and approx. 2.5M for the solid. Due to the central importance of conjugate heat transfer between the solid and the fluid, mesh fineness on the side of the fluid was increased at the interface to capture the thermal boundary layer. The overall cell size, measured as $\Delta x = \sqrt[3]{V_{\text{cell}}}$ varied from $5 \cdot 10^{-3}$ m in the boundary layer to 0.62 m in the bulk of the fluid subdomain (Fig. 7).

The fluid domain for the flame propagation simulation (*explosionDynamicsFOAM*) was discretized by an unstructured polyhedral grid with cell size distribution in the range between 0.1 m and 1 m, which is comparable to other CFD studies of full reactor containments in the literature, i.e. 0.22 m in Hasslberger et al. (2017b,a), 0.5 m – 1 m in Kang et al. (2020), 1 m in Hsu et al. (2014). The cell density was not increased near the walls, i.e., no boundary layer refinement was applied for the *explosionDynamicsFOAM*. The explanation lies in the fact that the central focus during the flame propagation stage is the gas volume's core, where the flame surface forms, as opposed to the containment structure surfaces where the flame extinguishes in contact with the solid. However, this modeling decision trades off a detailed prediction of turbulence generation in the boundary layers of specific parts of the containment, as discussed in Section 5. The unstructured polyhedral cells employed in this study enabled a highly efficient volume discretization, leading to the total cell count of about 650 000 (Figs. 6 and 7).

The gas distribution simulation with *containmentFOAM* achieved a second-order discretization of the cell gradients with the *linear* scheme, while the velocity gradient was discretized by the face-limited *linear* scheme (limiting factor 0.5). Spatial discretization of the momentum equation was achieved by blending the *linear* and *upwind* schemes with respect to the local velocity gradient. Spatial terms of enthalpy and species transport equations were discretized using the second-order *limited linear* scheme with the limiting factor of 1.0, while for the turbulence quantities k and ω, a first-order *upwind* scheme was applied. The Laplacian terms were discretized by the Gauss *linear* scheme, limited by a factor of 0.33. Temporal derivatives were discretized by a blend of 10% implicit Euler and 90% of Crank–Nicolson schemes (*Crank–Nicolson 0.9* in OpenFOAM settings).

In the flame propagation simulation with *explosionDynamicsFOAM*, the second-order least squares discretization scheme was used for cell gradient terms by default. Only for the gradient of the progress variable b, a cell-limited vertex-based Gauss method was used with multi-dimensional limiting and a limiting factor of 0.5. Advection of the conservative variables (ρ, ρU, ρE, ρb) was modeled by the all-speed high-resolution upwind scheme Advection Upwind Splitting Method (AUSM)$^+$up. Its application to a progress-variable-based combustion modeling of deflagrations was validated by Zivkovic and Sattelmayer (2021, 2023). The pressure and momentum diffusion coefficients of the AUSM$^+$up scheme were set to K_p = 0.25 and K_u = 0.75, while the limiting Mach number was M_{lim} = 0.1. The second-order bounded *SMART* scheme was used for face-cell reconstruction of physical variables by default, while the bounded version *SMART01* was used for the progress variable b. Advection of the turbulence variables k and ω in the flame propagation simulation was discretized by the second-order *limited linear* Gauss scheme with the limiting factor of 1.0. The diffusion (Laplacian) terms were handled in *explosionDynamicsFOAM* by Gauss linear second-order discretization.

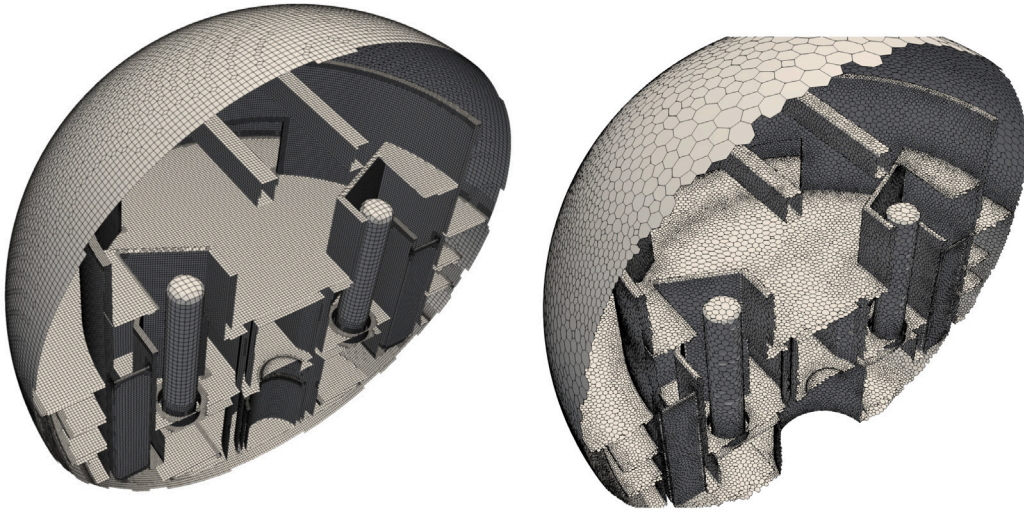

(a) (b)

Fig. 6. A Three-dimensional 3D view of the hexahedral-dominant mesh with boundary layer refinement used for the gas distribution simulation with *containmentFOAM* (a) and the unstructured polyhedral computational grid used for flame propagation simulation with *explosionDynamicsFOAM* (b).

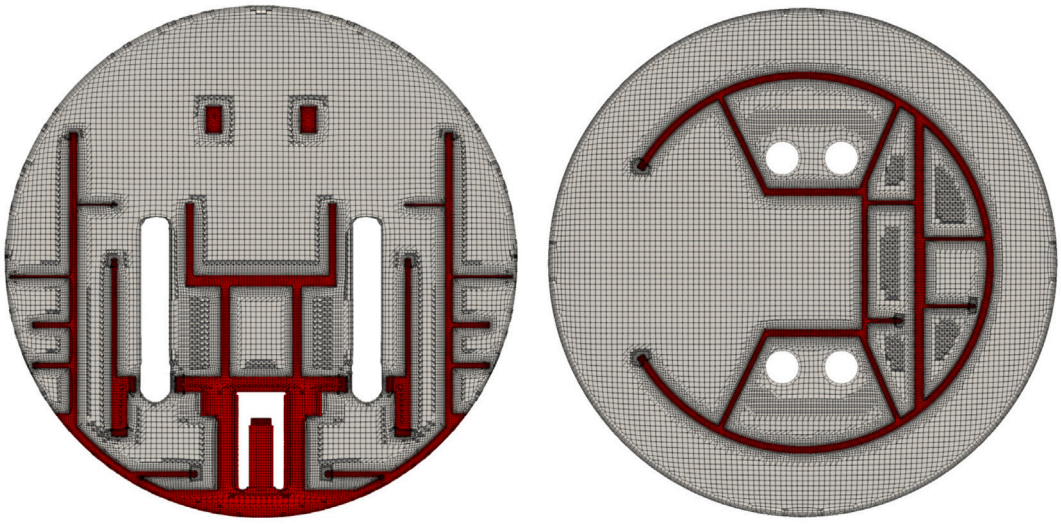

(a) X-Y plane. (b) Y-Z plane.

Fig. 7. Cut view of the hexahedral-dominant mesh with boundary layer refinement used for the gas distribution simulation with *containmentFOAM* with the fluid region grid in gray and solid region grid in red.

In the gas distribution simulation, the solution of the discretized equations was achieved in *containmentFOAM* by a maximum of 10 outer correctors of the PIMPLE algorithm, which consisted of solving equations for the fluid and solid domains. In the solid, the enthalpy equation was solved repeatedly using a Preconditioned Conjugate-Gradient (PCG) linear solver with the Diagonal-based Incomplete Cholesky (DIC) preconditioner to the absolute tolerance of 10^{-6}, until convergence of the initial residuals reached the tolerance of 10^{-4}. A single non-orthogonal corrector was applied in the inner solution loop. In the fluid subdomain, the equations for momentum, enthalpy, species transport and turbulence quantities (k and ω) were solved using the symmetric preconditioned bi-conjugate gradient (*PBiCGStab*) linear solver with the Diagonal-based Incomplete LU preconditioner (DILU). In contrast, the pressure equation was solved by the Generalized Geometric-Algebraic Multigrid (GAMG) with the Gauss–Seidel smoother. The absolute tolerance for the normalized residual was 10^{-6} for the pressure equation and 10^{-8} for other variables, while the relative tolerance was set to zero for all. The inner corrector loop for the fluid included two non-orthogonal correctors and was executed until either the initial residuals converged to the tolerance of 10^{-4} for all variables or the loop reached 20 executions. No under-relaxation was used, except for turbulence quantities (k, ω), which were under-relaxed by a factor of 0.9.

The *containmentFOAM* simulation was initialized by mapping *Generic Containment* COCOSYS results from t = 47:00 h of the accident. The mapping procedure used a Computer Aided Design (CAD) model of each individual LP zone (extracted from the CAD model of the containment), which was then used to select all cells of the 3D CFD grid enclosed within the surfaces of that zone. This was achieved using the OpenFOAM utility application `setFields` which takes the zone geometry (CAD file) and LP values as inputs and initializes the CFD cell values accordingly.

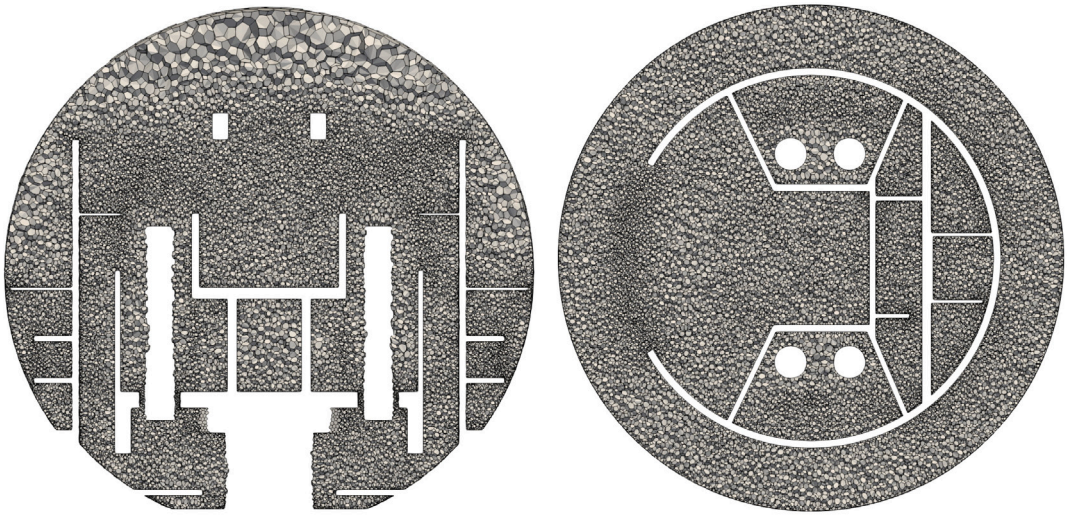

(a) X-Y plane. (b) Y-Z plane.

Fig. 8. Cut view of the polyhedral computational grid used for the flame propagation simulation with *explosionDynamicsFOAM*, consisting of only the fluid region.

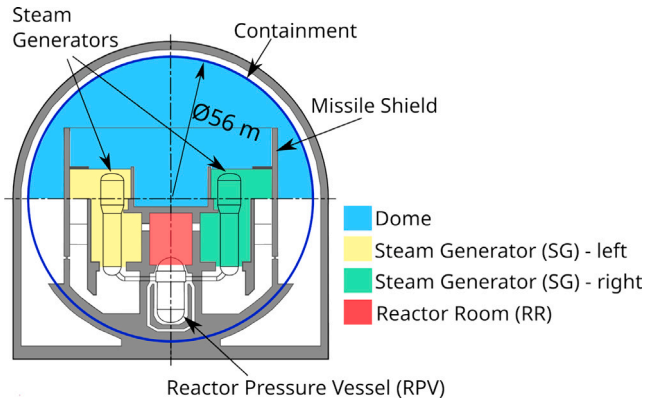

Fig. 9. Highlight of the containment compartments most important for the flame propagation phase: Dome, Steam Generators (SG) left & right and Reactor Room (RR).

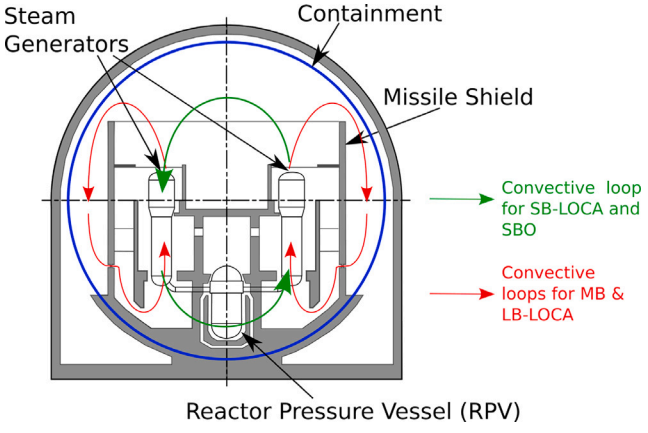

Fig. 10. Convection loops in the *Konvoi*-type reactor containment differ with the accident scenario: a single loop is closed in an SB–LOCA or an SBO, while a dual loop emerges in an MB- or an LB-LOCA.

The gas distribution CFD was run for about 5 min of physical time. The adjustable simulation time step was used with the upper limit for the advective CFL number of 10 (CFL = $\frac{|u_i|\Delta t}{\Delta x}$).

In flame propagation simulation using the density-based solver *explosionDynamicsFOAM* the governing equations are solved as a coupled set. The reaction progress variable b is solved by a passive scalar equation, with the heat release from combustion subsequently explicitly corrected in the mixture update. The turbulence variables k and ω are solved segregated from the Navier–Stokes equations using an implicit solver *PBiCGStab*, to the relative tolerance of 10^{-6}. The second-order time integration in *explosionDynamicsFOAM* is achieved with the SSP–Runge–Kutta (RK) method (Ketcheson, 2010) with the number of stages set to $m = 3$. The parameter m can be freely chosen so that, if increased, a greater stability is achieved, allowing for a greater time step size (and CFL) (Zivkovic and Sattelmayer, 2021). In the present work, the time step was chosen to satisfy the accuracy criterion, i.e., the acoustic CFL number ($CFL = \frac{(|u_i|+c)\Delta t}{\Delta x}$) condition was kept at unity for the entire duration of the flame propagation.

5. Results and discussion

5.1. Gas distribution

The simulation of thermal hydraulics and gas distribution inside the *Konvoi* containment with *containmentFOAM* obtained detailed spatial distributions for gas species concentrations, temperature, pressure, gas velocity and turbulence fields.

The containment compartments of primary interest for the combustible gas formation and subsequent flame propagation in the present study are depicted schematically in Fig. 9. More generally, the compartments can be subdivided into the *equipment rooms*, which include compartments within the missile shield and below the burst membranes of the steam generators, and the *operating compartments*, including the Dome and all other accessible areas.

The gas mixture in the CFD results (Fig. 11(a)) was found to be effectively homogeneous within the equipment rooms and the Dome. The observed mixture homogeneity is a direct consequence of the main convective circulation loop driven by buoyancy due to temperature differences. The loop is schematically depicted in Fig. 10 in green. Heat released from the MCCI process is transferred into the domain via the hot surface of the RPV head, resulting in a significant temperature

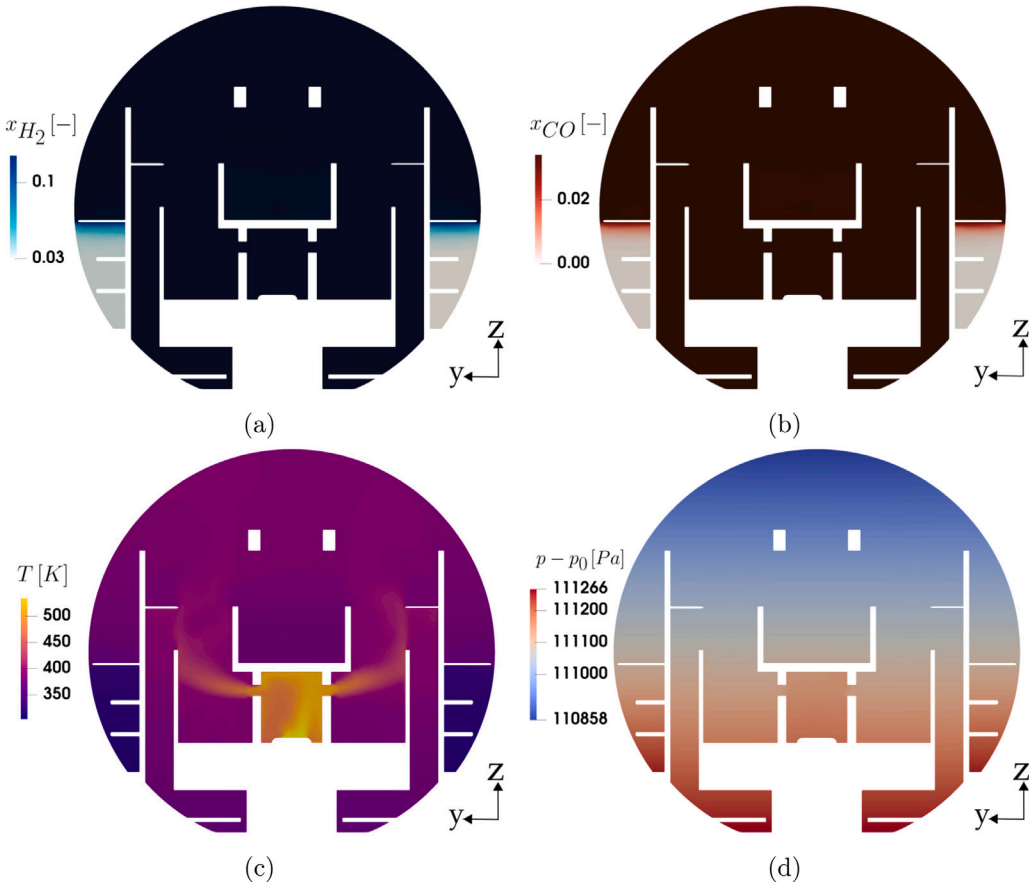

Fig. 11. Volume fractions (x_{H_2}, x_{CO}), temperature (T) and relative pressure (p - p_0) fields resulting from the *containmentFOAM* simulation used to initialize the flame propagation analysis with *explosionDynamicsFOAM*.

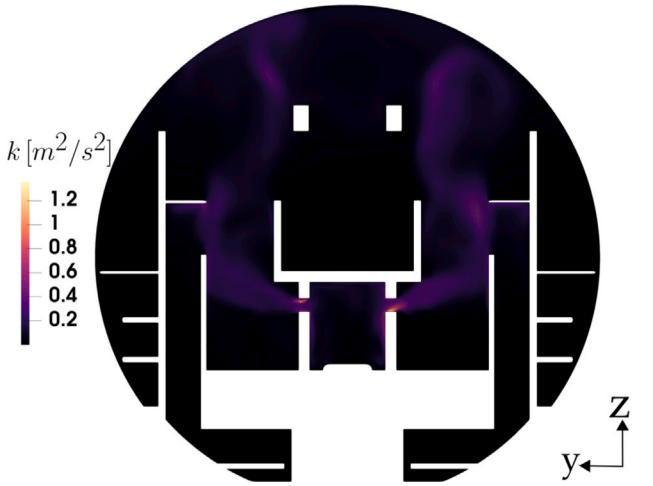

Fig. 12. Cut-view of the turbulence kinetic energy k initial conditions for the *Generic Containment* case flame propagation analysis.

rise inside the RR compartment and, in turn, a flow between the RR and SG compartments (Fig. 11). Consequently, the highest turbulence production is found at that same location.

The gas distribution results, i.e. the mixture homogeneity, is consistent with the other LP–CFD studies of PWR containments in similar accident conditions (Hasslberger et al., 2017b). In a PWR-type reactor containment, the establishment of convection loops is promoted by the plant design to achieve dilution of flammable gases. This strategy helps mitigate the local formation of rich fuel pockets, which could potentially increase the Flame Acceleration (FA) risk. This contrasts the BWR reactor types, where gases leaked from the inertized containment form a stratified layer in the reactor building (Manninen et al., 2000), which can lead to locally-rich flammable gas conditions that can cause a powerful explosion, e.g. as in the Fukushima–Daiichi accident (Xiao et al., 2017b).

The formation of the convective loops in the *Konvoi* containment (one vs. two loops) depends on the accident sequence, particularly the break size, which dictates pressure differentials and the number of burst membranes and doors opening. In a slow release (SB–LOCA or SBO), SG compartments' ceiling membranes are the only ones opening, resulting in a single convection loop. The second convective loop is formed in case of a MB- or a LB–LOCA, where the more pronounced pressure rise can additionally blow the doors in the missile shield out, allowing for an even stronger mixture homogenization (Sonnenkalb et al., 2015).

Moreover, in the scenario considered here, the CFD simulation of gas distribution was initialized at a late time in the accident (t = 47 h). At this stage, there are no further injections (mass sources) which could influence the local gas composition or the convection itself, at the same time, the temperature profiles of the structures (the solid domain in the CFD) have stabilized, together with the steam condensation rates, which are modest at that point. In such conditions, the described main convective loop is very effective in homogenizing the gas mixture.

The average gas velocity reached a steady ≈ 0.5 m/s in the main convective loop. At that rate, gas would have traveled around 150 m in the approx. 340 s (5 min) of the simulated time. This distance corresponds to roughly three full circulations of the containment diameter, which was judged as sufficient for the flow and turbulence fields to establish a quasi-steady state. Considering the stage of the accident, with no

Table 2
Locations of the pressure probes and the ignition point (cf. Fig. 13).

	Compartment	x [m]	y [m]	z [m]
Ignition	RR	−2.5	0	11
Pressure probe P1	RR	1	0	16
Pressure probe P2	SG left	0	12	16
Pressure probe P3	Dome	0	0	30

further mass sources and the near-constant heat source, a quasi-steady convection flow (with the inherent local fluctuations characteristic for buoyancy-driven flows) was reached.

Results of the *containmentFOAM* simulation in Fig. 11 represent the realistic initial state for the subsequent flame propagation analysis. A critically important output of the *containmentFOAM* from the perspective of the subsequent flame propagation simulation is the estimation of the turbulent kinetic energy (k) field due a potential influence of the turbulence on the flame dynamics. The turbulence was modeled using the k-ω SST model, which included the production and dissipation of turbulence due to buoyant forces. The results depicted in Fig. 12 show that the highest, albeit still low, turbulence levels were localized in the region where RR–SG connect (strong duct flow). Overall, the turbulent kinetic energy k field shows that turbulence production in the present scenario remains very low, with k remaining below 1.3 J/kg (m^2/s^2), which is insufficient to affect flame wrinkling. The pre-ignition turbulence assessment here represents a significant improvement over previous studies that typically lacked such data, i.e., most prior full-containment studies either assumed a fully turbulent regime or neglected it without quantification.

5.2. Ignition and flame propagation

The gas distribution simulation results from *containmentFOAM*, obtained in the prior step of the accident analysis chain, were mapped onto the unstructured polyhedral grid (Fig. 8) using the OpenFOAM's *mapFields* application. The grid was then used for the flame propagation simulation in *explosionDynamicsFOAM*. The pressure, temperature, gas composition, velocity and turbulence variables were all mapped and used as initial conditions for the *explosionDynamicsFOAM* simulation.

Ignition at the hot surface near the RPV head, close to the bottom of the Reactor Room (RR), was simulated by setting the reaction progress variable b to 0 (burned state). Fig. 13 shows the exact locations of the ignition point and the pressure probes. Their coordinates are specified in Table 2. The ignition location was selected based on several criteria. First, its high initial temperature (Fig. 11(c)) increases the likelihood of ignition. Second, it is located within a more confined part of the containment (RR), with previous studies demonstrating a higher flame acceleration potential proportional to geometrical confinement (Manninen et al., 2002; Hasslberger et al., 2017b). Finally, the length of the flow path in the vertical direction and an increased geometrical complexity along the flame path were demonstrated by Kim and Hong (2015) to increase the flame acceleration potential.

The flame propagation phase consists of two distinct parts. In the *early phase* (beginning with ignition at $t = 0$ s), the flame remains within the *equipment rooms*, i.e., RR and SG compartments (Fig. 9). The *late phase* begins at $t = 1.3$ s with the flame entering the *operating compartments*, specifically the Dome. The division corresponds to the change in the combustion process dynamics, as discussed in the following sections.

5.2.1. Early flame propagation phase ($t < 1.3$ s)

Following ignition, the flame kernel expanded hemispherically (Figs. 15 and 16 at $t = 0.4$ s) before reaching the RR compartment walls. Due to significant confinement in the RR geometry, which restricted the outflow to the SG compartments to only the two narrow ducts, the pressure within the RR began to rise sharply relative to the pressure in

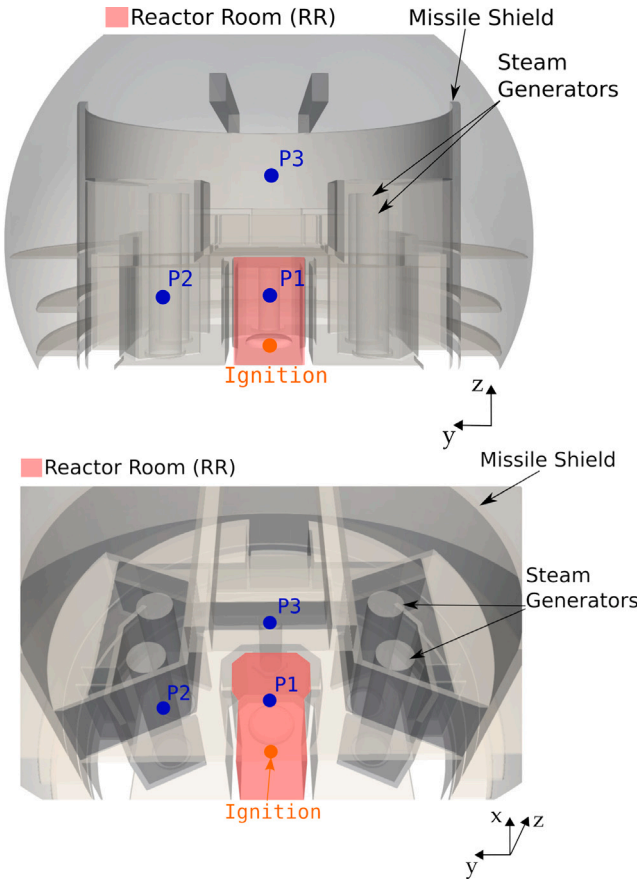

Fig. 13. Computational domain images including the ignition and pressure probe locations.

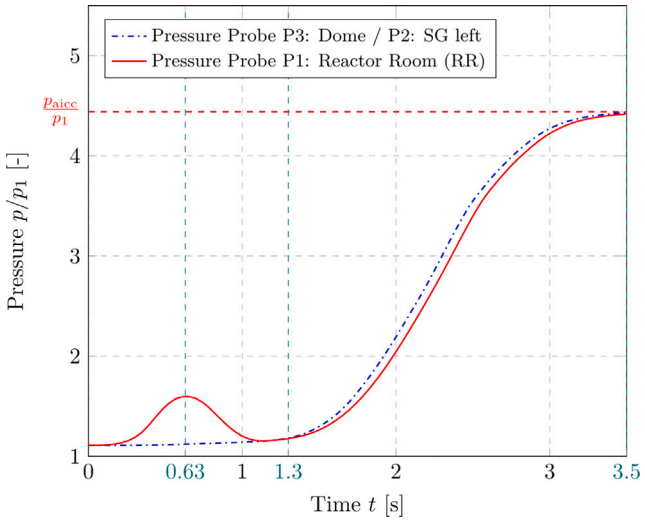

Fig. 14. Pressure probe readings showing the containment pressurization during the flame propagation phase.

the adjacent SG volumes, as indicated by probe P1 compared to P2/P3 in Fig. 14.

The quickly rising pressure difference between the RR and SG compartments drove high-velocity gas jets (reaching over 450 m/s, Fig. 17(a)) through the connecting ducts to emerge, accompanied by a significant elongation of the flame front. The flame entered the SG volumes (Figs. 15, 16) at approx. $t = 0.6$ s. By $t = 0.8$ s, the upwardly

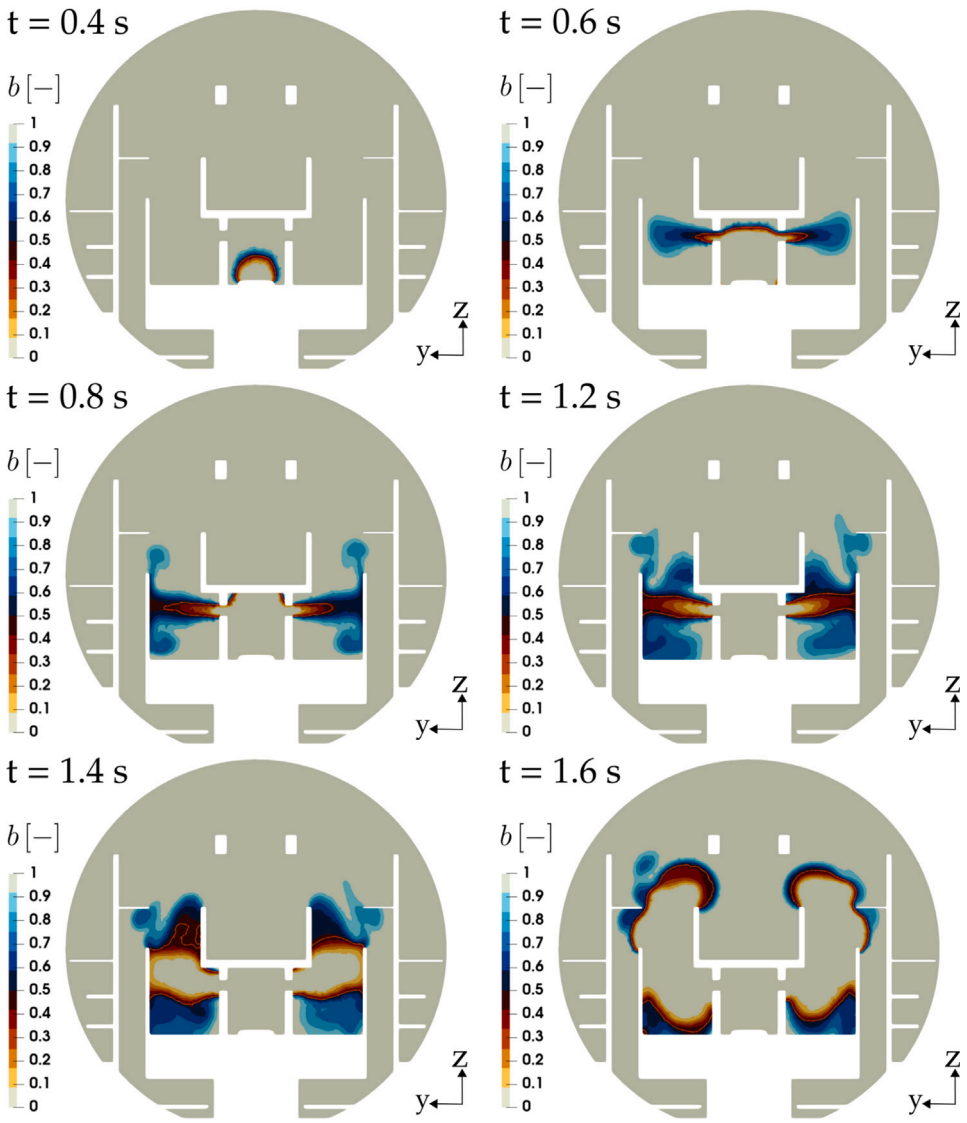

Fig. 15. Propagation of the flame front in the *early phase* of the combustion process. Gas jets passing through the two ventilation ducts connecting the RR and SG compartments are clearly visible at $t = 0.8$ s and $t = 1.2$ s.

propagating portion of the flame surface remaining in the RR had reached the compartment's top wall. Simultaneously, the duct jets impinged on the walls in the SG compartments, generating a localized, moderate overpressure region (approx. $\Delta p = 2000$ Pa, Fig. 18). The incoming gas jet formed a wall-attached flow pattern radial to the wall surface.

Fig. 15 shows that during periods of high gas velocity (from $t = 0.6$ s to $t = 1.4$ s), the reaction progress variable field (b) became more spread out, suggesting stronger diffusion by the flow, although the flame front remained thin in general. During this phase, the primary mechanisms for turbulence generation were identified as the jet-wall interaction behind the steam generators and shear stresses within the narrow ducts. The turbulent kinetic energy k peaked briefly at $k_{\max} \approx 50\,\mathrm{m^2/s^2}$ around $t = 0.8$ s – 1.0 s interval (17(b)) before dropping sharply to $k \approx 27\,\mathrm{m^2/s^2}$ by $t = 1.2$ s.

To evaluate the potential influence of the turbulence generated during the flame propagation on the flame acceleration, a comparative analysis was performed between the turbulent flame wrinkling for the peak turbulence kinetic energy (from $t = 0.8$ s to 1.0 s) estimated by the turbulent flame speed model of Goulier et al. (2017) and the wrinkling predicted by the instability-driven model (Zivkovic and Sattelmayer, 2023). The peak turbulent flame wrinkling was

$$\Xi_t = 1.61 \left(\frac{u_i'}{S_l}\right)^{0.526} \left(\frac{r}{L_t}\right)^{0.33} \mathrm{Le}^{-0.14}, \tag{1}$$

where the fluctuating velocity component u_i' relates to the turbulent kinetic energy k as

$$u_i' = \sqrt{\frac{2}{3}k}. \tag{2}$$

Since the maximum turbulent kinetic energy at the flame front surface (at $t = 0.8$ s) is

$$\max_{b=0.5} k = 44.5 \left[\frac{\mathrm{m^2}}{\mathrm{s^2}}\right], \tag{3}$$

and by assuming fully developed wrinkling ($\left(\frac{r}{L_t}\right) \to 0$), while omitting the Lewis number term due to $\mathrm{Le} = 1.2 > 1$, the $\max_{b=0.5} \Xi_t$ is

$$\max_{b=0.5} \Xi_t \approx 1.61 \left(\frac{\sqrt{\frac{2}{3} \cdot 44.5}}{0.74}\right)^{0.526} = 4.6\,[\text{-}]. \tag{4}$$

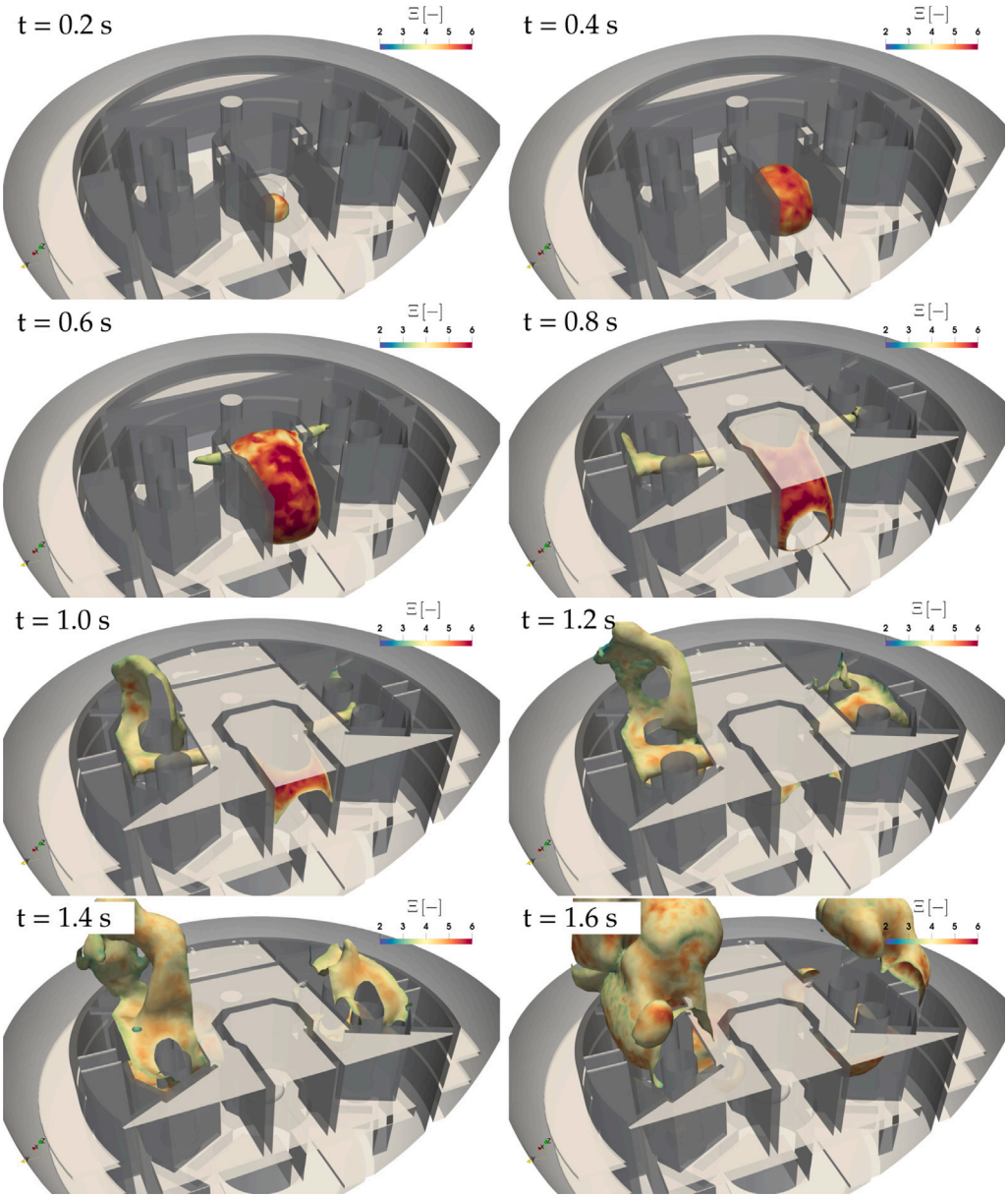

Fig. 16. Transient progression of the flame isosurface ($b = 0.5$) in the *early phase* of flame propagation, with the Ξ field quantifying the flame wrinkling.

The turbulent model by Goulier et al. (2017) used here was considered particularly suitable given it was validated for H_2–CO mixtures and moderate turbulence intensity (Desclaux et al., 2022). The instability-driven wrinkling model by Zivkovic and Sattelmayer (2023) predicted the maximum wrinkling factor of

$$\max_{b=0.5} \Xi_{\text{inst}} = 4.73\ [\text{-}] \tag{5}$$

at the corresponding time and location. The maximum wrinkling factor comparison suggests that the turbulence generated during the flame propagation phase, as far as it was resolved by the simulation, was insufficient to significantly increase the flame wrinkling beyond the dominant effect of the Darrieus–Landau instability. It must be noted, however, that due to a coarse grid resolution, the simulation was likely unable to sufficiently resolve the turbulence generation within the shear layers of the jet flow and at the walls. Nonetheless, the simulation highlights the critical areas of turbulence generation in the flame propagation phase inside a *Konvoi* reactor containment. A higher-resolution CFD study of the region around the RR–SG duct is necessary to further quantify the turbulence generation and its influence on the flame speed.

The flame completely encircles the steam generators no later than $t = 1.3$ s, spreading upward and downward in the SG compartment after impacting the wall opposite the ducts, with a stronger upward tendency due to buoyancy. The consumption of the remaining reactants in the RR and SG compartments marked the completion of the flame propagation phase within the *equipment rooms* around that time (Figs. 15, 16).

5.2.2. *Late flame propagation phase ($t > 1.3$ s)*

The beginning of the *late phase* of the flame propagation process is marked by the flame entering the Dome compartment from the two SG compartments at approximately $t = 1.3$ s.

The combustion rate increased upon the flame entering a large, open volume of the Dome. Once released from the geometric constraints of the inner compartments, the flame surface area underwent rapid expansion. At this time, an inflection point can be observed in the overall combustion progress plot in Fig. 19, showing a rapid acceleration in the consumption rate of the unburned mixture. While the local flame

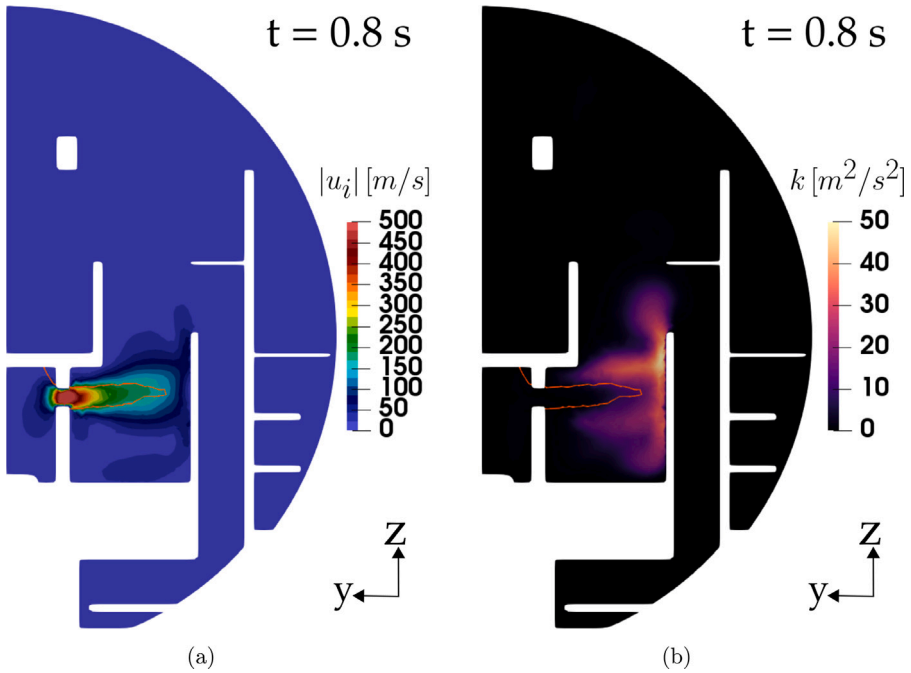

Fig. 17. Gas jet at the moment when the peak pressure is reached in the Reactor Room (RR) compartment (a). A flame elongation is observed due to the strong advection, illustrated by the isoline $b = 0.5$, marked in orange. The turbulent kinetic energy generation in the shear layer and after impingement is depicted in (b).

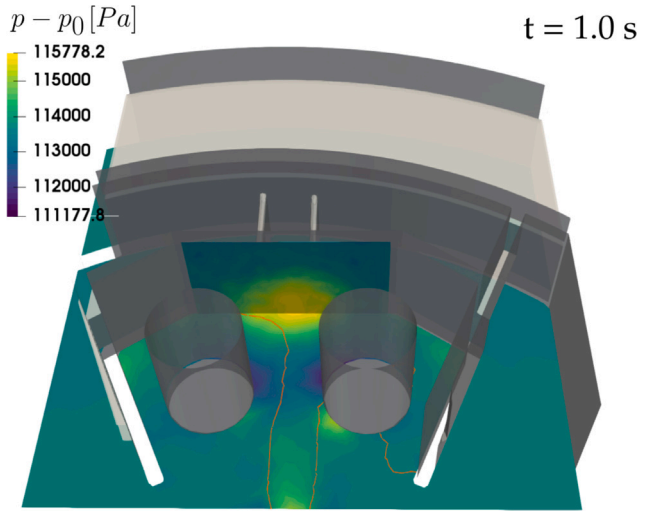

Fig. 18. Pressure field at the location of gas jet impingement ($t = 1$ s) in the steam generator compartment shows a moderate overpressure (≈ 2000 Pa). The flame (isoline $b = 0.5$) location is shown as an orange line.

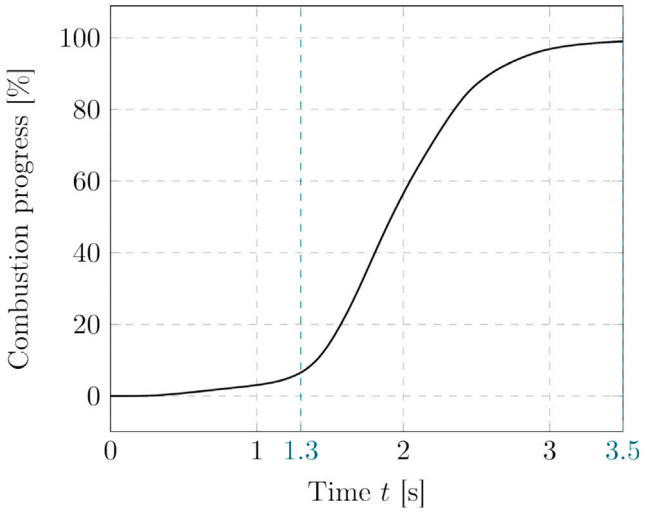

Fig. 19. Percentage of burned flammable gas volume in the containment over time.

speed decreased compared to the *equipment rooms* due to the lack of confinement, the rapid increase in flame surface area resulted in an increased overall volumetric burning rate. These findings correspond to comparable studies conducted on large dry-volume PWR containments, as shown by Kim and Hong (2015) and Hasslberger et al. (2017a).

Consequently, the overall pressure rise in the containment accelerated significantly (Fig. 14, probes P2 and P3 after $t = 1.3$ s). By $t = 2$ s, the initial overpressure had doubled, with approximately 35% of the flammable mixture combusted. The rate of pressure rise in the RR (Probe P1) became comparatively slower than in the Dome/SG, as the RR was now being pressurized by backflow from the combustion occurring in the *operating compartments*. The combustion process advanced rapidly, reaching 80% completion by $t = 2.5$ s.

The flame propagated predominantly upwards after entering the Dome. Initially, two parallel flame structures emerged from the SG compartments, joining near the Dome centerline around $t = 2.0$ s (Figs. 20, 21). The flame front continued its upward trajectory, reaching the apex of the Dome around $t = 2.6$ s (Fig. 21). A portion of the flame front bifurcated, entering the annular space outside the missile shield. The simulation was complete at $t = 3.5$ s.

Fig. 19 shows combustion progress in terms of the flammable gas consumption. When the complete combustion of flammable gas is reached, the pressure reaches the adiabatic isochoric complete combustion pressure p_{aicc} of the gas mixture.

At no point during the flame propagation phase does the predicted flame wrinkling Ξ reach levels which could lead to either a fast deflagration (flame propagating at sonic speed) or a DDT. The fundamental

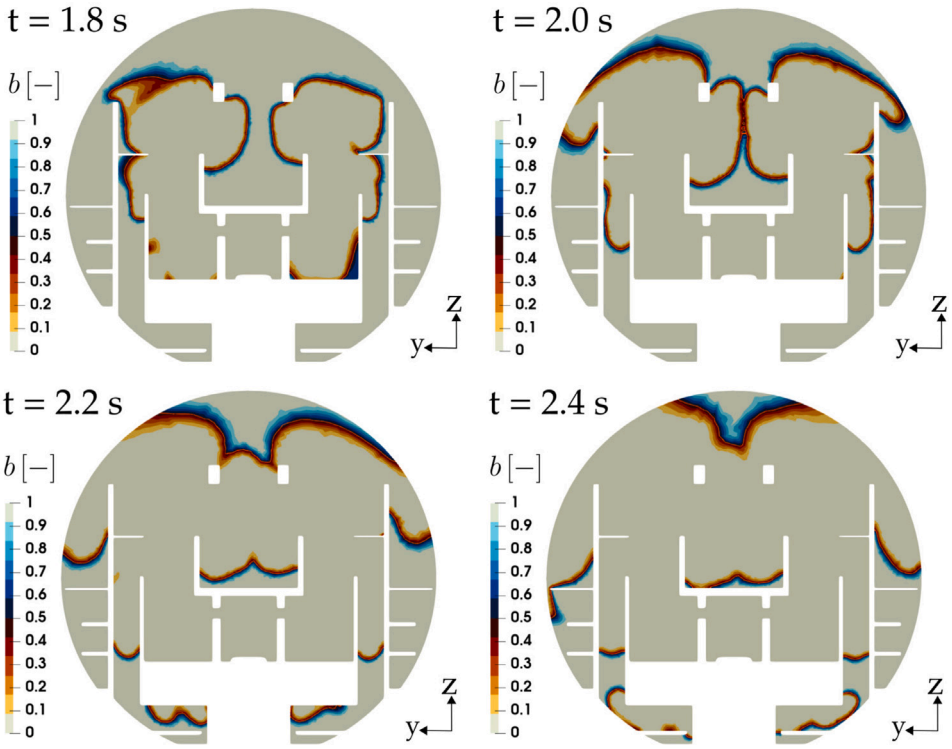

Fig. 20. Propagation of the flame in the Dome compartment, once it leaves the *equipment rooms* in the *late phase* of the combustion process.

Table 3
Computational cost.

	Simulated time	Core hours
COCOSYS	47 h	20
containmentFOAM	≈ 345 s	9200
explosionDynamicsFOAM	3.5 s	21 500

flame speed (in the frame of reference of unburned gas) reaches its maximum at

$$\max\left(S_{\text{eff}}\right) = \Xi_{\max} \cdot S_{\text{l}} = 17.8 \cdot 0.74 = 13.2 \ \frac{\text{m}}{\text{s}}, \tag{6}$$

resulting in the observable flame speed (in the stationary frame of reference) of $V_{\max} = 456.7\,\text{m/s}$, significantly lower than the Chapman–Jouguet (CJ) detonation velocity for the considered case of $V_{\text{cj}} \approx 1712\,\text{m/s}$. Taking into account that a deflagration typically needs to accelerate to roughly half the CJ velocity to trigger DDT in smooth tubes (Lee, 2008), the simulated flame acceleration can be considered insufficient for DDT through shock-flame coupling.

5.3. Computational cost

The computational cost of the LP and CFD simulations is presented in the following. The COCOSYS simulation of the 47 h transient took ≈ 20 h on a single CPU core. The *containmentFOAM* CFD simulation of ≈ 5 min required ≈ 3 days of compute time on a 128-core Xeon Gold CPU node. The flame propagation phase lasting 3.5 s required ≈ 14 days to compute on a 64-core CPU node with two AMD EPYC 7502 32-core CPUs. Table 3 shows the breakdown of the computational cost expressed in CPU core hours. The results underline the necessity of LP modeling for generating the initialization data for CFD, especially in the present scenario where ignition occurs at a late stage of the accident.

A substantial difference in the computational cost, when considering the simulated time interval, between two CFD solvers results from the difference in the required temporal accuracy. The flame propagation, simulation with *explosionDynamicsFOAM*, was limited by the acoustic Courant (CFL = $\frac{(|u_i|+c)\Delta t}{\Delta x}$) number due to a general requirement of resolving fast pressure waves that might lead to shocks, which, in turn, might lead to DDT, neither of which was possible to rule out beforehand given that the final gas mixture is in the potentially detonable range. In contrast, the thermal-hydraulics simulation with *containmentFOAM* was able to use a PISO-SIMPLE solver algorithm, allowing for a kinematic CFL criterion ($CFL = \frac{(|u_i|)\Delta t}{\Delta x}$). For more details on the numerical methods of the two solvers see Section 2.

6. Summary & conclusions

The present work successfully demonstrated a comprehensive nuclear reactor accident analysis chain, integrating Lumped Parameter (LP) simulations with full-scale CFD analyses for both gas distribution and subsequent combustion phases. The workflow was applied to an SB–LOCA scenario within the *Generic Containment* (derived from a *Konvoi*-type PWR), providing detailed insights into the potential consequences of the considered accident event.

First, LP data from a COCOSYS simulation were used to initialize the *containmentFOAM* CFD simulation of gas mixing. LP codes like COCOSYS offer an efficient computational method for modeling the follow-up of a reactor accident, with key accident stages that may extend over several days. Furthermore, COCOSYS includes sub-models for critical phenomena such as reactor core melting, steam evaporation, and condensation, along with the behavior of the safety systems that could affect the progression of the accident.

The CFD code *containmentFOAM*, developed and validated for thermal-hydraulic conditions of a LOCA, was applied to simulate the final gas mixing state prior to ignition, i.e., to compute gas composition, pressure, velocity, and turbulence fields that allowed the subsequent flame propagation CFD with *explosionDynamicsFOAM* to start with significantly more realistic initial conditions, thus making an important step beyond traditional approaches relying on simplified assumptions such as equivalent stoichiometric clouds or direct initialization with LP results. The present work introduced a reactor accident combustion CFD analysis that was initialized with a spatially resolved turbulence

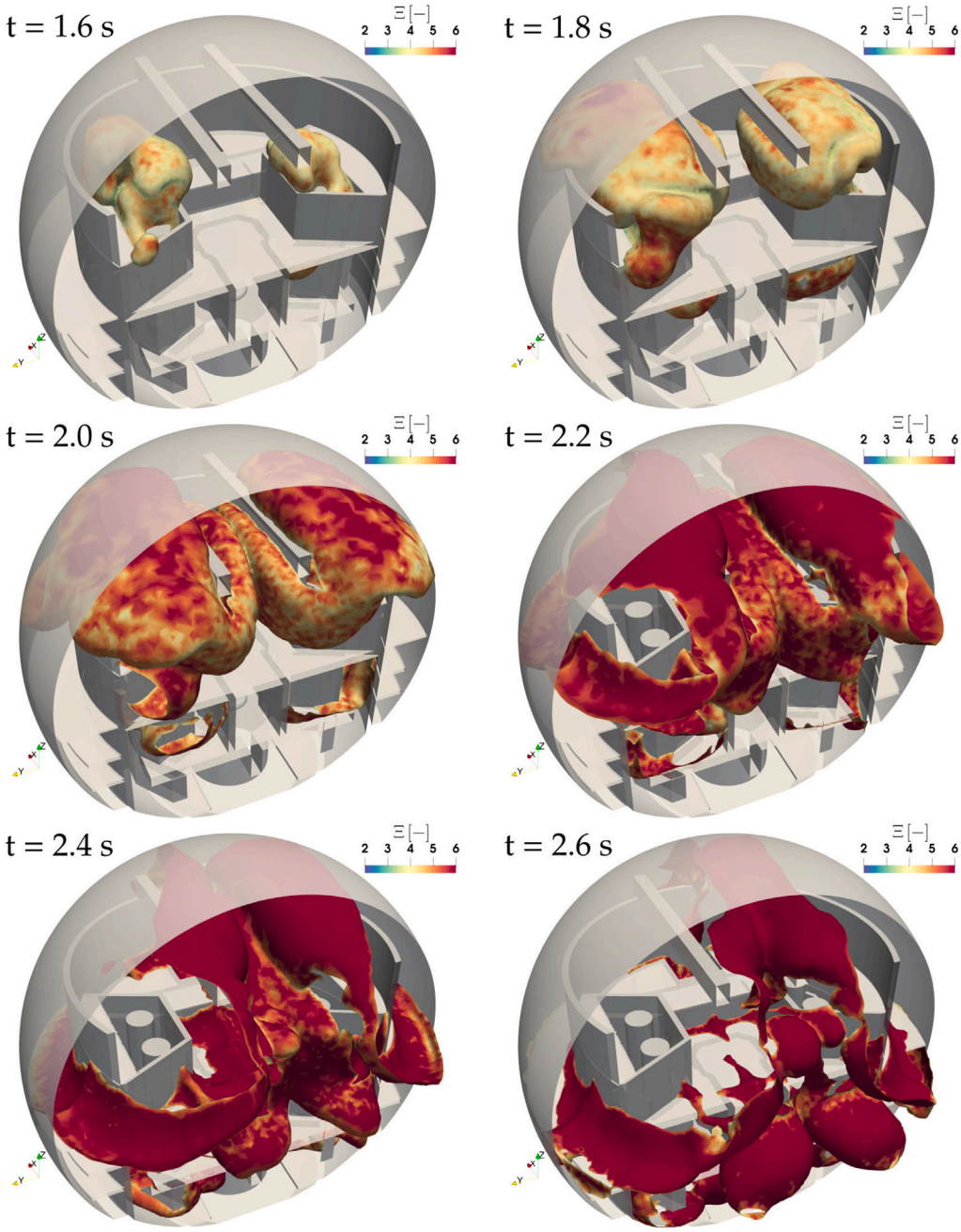

Fig. 21. Transient progression of the flame isosurface ($b = 0.5$) in the *late phase* of flame propagation, with the Ξ field quantifying the flame wrinkling.

intensity field. For the considered scenario, the initial turbulence levels were predicted to be low, a key finding that directly informed the combustion modeling strategy, unlike the prior studies in the literature, which largely assumed a fully-developed turbulent regime.

The final step of the analysis chain was the flame propagation simulation, performed using *explosionDynamicsFOAM*, which provided valuable insights into the combustion dynamics. The simulation successfully captured complex, geometry-influenced flow phenomena, including the initial confinement effects within the Reactor Room (RR), the formation of high-velocity jets into the Steam Generator (SG) compartments, and the subsequent expansion into the unconfined Dome volume. The results also quantified the most relevant variables for safety considerations, i.e., the peak pressure, overall combustion rate, and the maximum flame speed.

The low initial turbulence resulted in the use of a scale-adaptive, instability-driven flame wrinkling model appropriate for the quasi-laminar conditions encountered at ignition. While turbulence generation was predicted in the simulation — particularly in areas of high confinement and high gas velocity, its predicted intensity was insufficient to increase the flame wrinkling beyond the dominant Darrieus–Landau (DL) instability effects for the analyzed case.

Ultimately, the assessment of the simulated flame propagation indicated a slow deflagration regime throughout the containment volume. The analysis revealed that the flame acceleration achieved under these specific SB–LOCA conditions was insufficient to meet the criteria for DDT. The maximum temperature load in the present work was the adiabatic flame temperature (approx. 2200 K), while the local pressure loads remained moderate, with the peak dynamic overpressure resulting from jet impingement of approximately 2278 Pa.

The coupled analysis chain presented here provides a robust yet flexible framework for incorporating more detailed physics into nuclear safety analysis, paving the way for safety assessment tools that allow a deeper understanding of severe accident phenomena. While the demonstrated integrated workflow represents a significant step toward a more realistic safety assessment, notable limitations remain. The use of coarse computational grids, necessary for full-scale containment simulations, likely resulted in an under-prediction of peak turbulence. Therefore, a detailed simulation that would resolve the shear stresses of the jet flow in and around the RR–SG duct should be conducted in the future work. Initialization of CFD analysis remains critically dependent on mapping results from the computationally less expensive simulations done with LP tools. A manual mapping procedure of the LP output onto the CFD grid was viable in the present work due to a coarse LP nodalization. However, it may be beneficial for the productivity and reliability of the accident analysis chain that the future work deals with developing a more automated workflow for that purpose.

Nomenclature

Acronyms

3D	Three-dimensional
AUSM	Advection Upwind Splitting Method
BWR	Boiling Water Reactor
CAD	Computer Aided Design
CFD	Computational Fluid Dynamics
CFL	Courant–Friedrich–Lewy
CJ	Chapman–Jouguet
COCOSYS	Containment Code System
DDT	Deflagration-to-detonation Transition
DL	Darrieus–Landau
EBU	Eddy Break-up
EDC	Eddy-Dissipation Combustion
FA	Flame Acceleration
FVM	Finite Volume Method
GRS	Gesellschaft für Anlagen- und Reaktorsicherheit gGmbH
LB	Large Break
LOCA	Loss of Coolant Accident
LP	Lumped Parameter
MB	Medium Break
MCCI	Molten Corium Concrete Interaction
PAR	Passive Autocatalytic Recombiner
PaSR	Partially Stirred Reactor
PWR	Pressurized Water Reactor
RANS	Reynolds-averaged Navier–Stokes
RK	Runge–Kutta
RPV	Reactor Pressure Vessel
RR	Reactor Room
SAMHYCO-NET	Severe Accident Mitigation by Hydrogen Control – Network
SAS	Scale Adaptive Simulation
SB	Small Break
SBO	Station Black-out
SG	Steam Generator
SSP	Strong Stability Preserving
SST	Shear Stress Transport
TD	Thermal–difussive
TFC	Turbulent Flame Closure
URANS	Unsteady Reynolds-averaged Navier–Stokes

Symbols

S_l	laminar flame speed (m/s)
T	temperature (K)
b	reaction regress variable (-)
c	speed of sound (m/s)
k	specific turbulent kinetic energy (m^2/s^2)
m	SSP Runge–Kutta scheme parameter (number of stages) (-)
p_0	containment pressure prior to the accident (Pa)
p_1	containment pressure at $t = 47$ h, the final pressure of the LP simulation (Pa)
p	pressure (Pa)
r	radius (m)
t	time (s)
u_i'	velocity fluctuation (Reynolds decomposition) (m/s)
x	volume fraction (-)

Greek symbols

Δx	cell size (m)
Ξ	flame wrinkling factor (-)
μ	dynamic viscosity (kg/(m s))
ω	turbulence eddy frequency(1/s)
ψ	relative humidity (-)

Subscripts

aicc	adiabatic isochoric complete combustion
eff	effective
l	laminar
t	turbulent

CRediT authorship contribution statement

Dario Živković: Writing – review & editing, Writing – original draft, Visualization, Validation, Software, Methodology, Investigation, Conceptualization. **Stephan Kelm:** Writing – review & editing, Validation, Software, Methodology, Investigation, Conceptualization. **Thomas Sattelmayer:** Writing – review & editing, Supervision, Project administration, Funding acquisition.

Declaration of competing interest

The authors declare that they have no known competing financial interests or personal relationships that could have appeared to influence the work reported in this paper.

Acknowledgments

This work was funded by the German Federal Ministry for the Environment, Climate Action, Nature Conservation and Nuclear Safety (BMUKN) based on a decision by the German Bundestag (Project no. 1501573), which is gratefully acknowledged. The simplified geometry of a *Konvoi* containment was provided by Dr. Jörn Stewering from the GRS. The LP results from GRS's code package AC2, specifically COCOSYS v2.4, were provided by Dr.-Ing. Michael Klauck (FZJ). Both of which the authors gratefully appreciate.

Data availability

Data will be made available on request.

References

Baraldi, D., Heitsch, M., Wilkening, H., 2007. CFD simulations of hydrogen combustion in a simplified EPR containment with CFX and REACFLOW. Nucl. Eng. Des. 237 (15–17), 1668–1678.

Bentaïb, A., Meynet, N., Bleyer, A., 2015. Overview on hydrogen risk research and development activities: methodology and open issues. Nucl. Eng. Technol. 47 (1), 26–32.

Bönigke, G., Ewig, F., Friedrichs, H., Heitsch, M., Hüttermann, B., Jendrich, U., Meier, S., Scharfe, A., Sonnenkalb, M., Rohde, J., 1998. Contributions to elaboration of concept and measures for optimized management of beyond-design-basis accidents in German LWR power plants; Untersuchungen von Maßnahmen des anlageninternen Notfallschutzes zur Schadensbegrenzung für LWR. Technical Report GRS-A-2601, GRS.

Bray, K., Libby, P.A., 1986. Passage times and flamelet crossing frequencies in premixed turbulent combustion. Combust. Sci. Technol. 47 (5–6), 253–274.

Bray, K., Moss, J., 1977. A unified statistical model of the premixed turbulent flame. Acta Astronaut. 4 (3–4), 291–319.

Breitung, W., Chan, C., Dorofeev, S., Eder, A., Gerland, B., Heitsch, M., Klein, R., Malliakos, A., Shepherd, J., Studer, E., 2000. Flame Acceleration and Deflagration-to-Detonation Transition in Nuclear Safety. Technical Report No. NEA/CSNI, Organisation for Economic Co-operation and Development, Paris, France.

Breitung, W., Royl, P., 2000. Procedure and tools for deterministic analysis and control of hydrogen behavior in severe accidents. Nucl. Eng. Des. 202 (2–3), 249–268.

Chase, M.W., 1998. NIST-JANAF Thermochemical Tables, vol. 9, American Chemical Society Washington, DC.

Chaudhuri, S., Akkerman, V., Law, C.K., 2011. Spectral formulation of turbulent flame speed with consideration of hydrodynamic instability. Phys. Rev. E 84 (2), 026322.

Chomiak, J., Lipatnikov, A.N., 2023. Simple criterion of importance of laminar flame instabilities in premixed turbulent combustion of mixtures characterized by low Lewis numbers. Phys. Rev. E 107, 015102.

Chung, W., Devaud, C.B., 2008. Buoyancy-corrected k–ϵ models and large eddy simulation applied to a large axisymmetric helium plume. Internat. J. Numer. Methods Fluids 58 (1), 57–89.

Daudey, N., Champassith, A., 2014. Accidental hydrogen release inside a nuclear power plant: CFD modelling and consequence analysis. In: 10th International Symposium on Hazards, Prevention and Mitigation of Industrial Explosions. ISHPMIE 10, Bergen, Norway.

Desclaux, A., Idir, M., Comandini, A., Bleyer, A., Bentaïb, A., Chaumeix, N., 2022. Experimental study on turbulent flame speed of H2-CO/air mixtures relevant to late phase accident scenario. In: 28th International Colloquium on the Dynamics of Explosions and Reactive Systems. ICDERS 28, Naples, Italy.

Dimmelmeier, H., Eyink, J., Movahed, M.-A., 2012. Computational validation of the EPR™ combustible gas control system. Nucl. Eng. Des. 249, 118–124.

Dinkelacker, F., Manickam, B., Muppala, S., 2011. Modelling and simulation of lean premixed turbulent methane/hydrogen/air flames with an effective Lewis number approach. Combust. Flame 158 (9), 1742–1749.

Fiorina, C., Clifford, I., Kelm, S., Lorenzi, S., 2022. On the development of multi-physics tools for nuclear reactor analysis based on OpenFOAM: state of the art, lessons learned and perspectives. Nucl. Eng. Des. 387, 111604.

Fuller, E.N., Schettler, P.D., Giddings, J.C., 1966. New method for prediction of binary gas-phase diffusion coefficients. Ind. Eng. Chem. 58 (5), 18–27.

Goulier, J., Comandini, A., Halter, F., Chaumeix, N., 2017. Experimental study on turbulent expanding flames of lean hydrogen/air mixtures. Proc. Combust. Inst. 36 (2), 2823–2832.

Hasslberger, J., Katzy, P., Boeck, L.R., Sattelmayer, T., 2017b. Computational fluid dynamics simulation of deflagration-to-detonation transition in a full-scale Konvoi-type pressurized water reactor. J. Nucl. Eng. Radiat. Sci. 3 (4), 041014.

Hasslberger, J., Kim, H.K., Kim, B.J., Ryu, I.C., Sattelmayer, T., 2017a. Three-dimensional CFD analysis of hydrogen-air-steam explosions in APR1400 containment. Nucl. Eng. Des. 320, 386–399.

Howell, J.R., Mengüç, M.P., Daun, K., Siegel, R., 2020. Thermal Radiation Heat Transfer. CRC Press.

Hsu, W.-S., Chen, H.-P., Lin, H.C., 2014. Hydrogen behavior in a large-dry pressurized water reactor containment building during a severe accident. In: 10th International Symposium on Hazards, Prevention and Mitigation of Industrial Explosions. ISHPMIE 10, Bergen, Norway.

Kampili, M., Kelm, S., Allelein, H., 2018. Modeling of aerosol transport and decay heat distribution in containment flows. In: Proceedings of the OECD/NEA & IAEA Workshop on Experiments and CFD Codes Application to Nuclear Reactor Safety. CFD4NRS-7, Shanghai, China, pp. 4–6.

Kampili, M., Vijaya Kumar, G., Kelm, S., Arul Prakash, K., Allelein, H.-J., 2021. CFD simulations of stratified layer erosion in MiniPanda facility using the tailored CFD solver containmentFOAM. Int. J. Heat Mass Transfer 178, 121568.

Kang, H.-S., Kim, J., Hong, S.-W., 2022. Numerical analysis for hydrogen flame acceleration during a severe accident initiated by SB-LOCA in the APR1400 containment. Hydrogen 3 (1), 28–42.

Kang, H.S., Kim, J., Hong, S.W., Kim, S.B., 2020. Numerical analysis for hydrogen flame acceleration during a severe accident in the APR1400 containment using a multi-dimensional hydrogen analysis system. Energies 13 (22).

Katzy, P., 2021. Combustion Model for the Computation of Flame Propagation in Lean Hydrogen-Air Mixtures at Low Turbulence (Ph.D. thesis). Technical University of Munich (TUM).

Katzy, P., Hasslberger, J., Sattelmayer, T., 2017a. On the effect of pressure on intrinsic flame instabilities in lean hydrogen-air mixtures Part II: Experimental investigation based on OH-PLIF technique. In: 26th International Colloquium on the Dynamics of Explosions and Reactive Systems. ICDERS 26, Boston, USA.

Kelm, S., Kampili, M., Liu, X., George, A., Schumacher, D., Druska, C., Struth, S., Kuhr, A., Ramacher, L., Allelein, H.-J., Prakash, K.A., Kumar, G.V., Cammiade, L.M.F., Ji, R., 2021a. The tailored CFD package 'containmentFOAM' for analysis of containment atmosphere mixing, H2/CO mitigation and aerosol transport. Fluids 6 (3), 100.

Kelm, S., Klauck, M., Beck, S., Allelein, H.J., Preusser, G., Sangiorgi, M., Klein-Hessling, W., Bakalov, I., Bleyer, A., Bentaïb, A., Kljenak, I., Stempniewicz, M., Kostka, P., Morandi, S., Ada del Corno, B., Bratfisch, C., Risken, T., Denk, L., Parduba, Z., Paci, S., Manfredini, A., Silde, A., Juris, P., Jancovic, J., Lele, H.G., Ganju, S., 2014. Generic Containment: Detailed comparison of containment simulations performed on plant scale. Ann. Nucl. Energy 74, 165–172.

Kelm, S., Müller, H., Allelein, H.-J., 2019. A review of the CFD modeling progress triggered by ISP-47 on containment thermal hydraulics. Nucl. Sci. Eng. 193 (1–2), 63–80.

Ketcheson, D.I., 2010. Runge-Kutta methods with minimum storage implementations. J. Comput. Phys. 229 (5), 1763–1773.

Kim, J., Hong, S.-W., 2015. Analysis of hydrogen flame acceleration in APR1400 containment by coupling hydrogen distribution and combustion analysis codes. Prog. Nucl. Energy 78, 101–109.

Kumar, G.V., Kampili, G.M., Kelm, S., Arul Prakash, K., Allelein, H.-J., 2019. Development and verification of a multi-species gas transport solver. In: Proceedings of the 14th OpenFOAM Workshop, Duisburg-Essen, Germany. pp. 23–26.

Lee, J.H.S., 2008. The Detonation Phenomenon. Cambridge University Press, Cambridge.

Lemmon, E.W., 2010. Thermophysical properties of fluid systems. In: NIST Chemistry Webbook. National Institute of Standards and Technology.

Li, X., You, X., Wu, F., Law, C.K., 2015. Uncertainty analysis of the kinetic model prediction for high-pressure H2/CO combustion. Proc. Combust. Inst. 35 (1), 617–624.

Lipatnikov, A., 2012. Fundamentals of Premixed Turbulent Combustion. CRC Press.

Liu, X., Kelm, S., Kampili, M., Kumar, G.V., Allelein, H.-J., 2022. Monte Carlo method with SNBCK non-gray gas model for thermal radiation in containment flows. Nucl. Eng. Des. 390, 111689.

Liu, F., Sun, Z., Ding, M., Bian, H., 2021. Research progress of hydrogen behaviors in nuclear power plant containment under severe accident conditions. Int. J. Hydrog. Energy 46 (73), 36477–36502.

Manninen, M., Lindholm, I., Huhtanen, R., Sjövall, H., 2000. Hydrogen in BWR reactor building. In: 8th International Conference on Nuclear Engineering. ICONE 8, American Society of Mechanical Engineers (ASME), Baltimore, USA, pp. 273–284.

Manninen, M., Silde, A., Lindholm, I., Huhtanen, R., Sjövall, H., 2002. Simulation of hydrogen deflagration and detonation in a BWR reactor building. Nucl. Eng. Des. 211 (1), 27–50.

Menter, F.R., Egorov, Y., 2010. The scale-adaptive simulation method for unsteady turbulent flow predictions. Part I: Theory and model description. Flow Turbul. Combust. 85 (1), 113–138.

Poinsot, T., Veynante, D., 2005. Theoretical and Numerical Combustion. R.T. Edwards.

Sonnenkalb, M., Band, S., Nowack, H., Schwarz, S., 2015. Re-evaluation of PAR concept in German PWR with revised PAR model. In: 16th International Topical Meeting on Nuclear Reactor Thermal Hydraulics. NURETH 16, Chicago, USA.

Sutherland, W., 1893. LII. The viscosity of gases and molecular force. Lond. Edinb. Dublin Philos. Mag. J. Sci. 36 (223), 507–531, Publisher: Taylor & Francis.

Travis, J., Spore, J., Royl, P., Lam, K., Wilson, T., Müller, C., Necker, G., Nichols, B., Redlinger, R., 1998. GASFLOW: A computational fluid dynamics code for gases, aerosols, and combustion. Vol. I Theory Comput. Model. Rep. FZKA-5994, la-13357-M.

Verein deutscher Ingenieure, 2013. VDI Wärmeatlas. Springer.

Vijaya Kumar, G., Cammiade, L.M.F., Kelm, S., Arul Prakash, K., Gross, E.M., Allelein, H.-J., Kneer, R., Rohlfs, W., 2021. Implementation of a CFD model for wall condensation in the presence of non-condensable gas mixtures. Appl. Therm. Eng. 187, 116546.

Weller, H., Tabor, G., Gosman, A., Fureby, C., 1998b. Application of a flame-wrinkling LES combustion model to a turbulent mixing layer. Symp. (Int.) Combust. 27 (1), 899–907.

Weller, H.G., Tabor, G., Jasak, H., Fureby, C., 1998. A tensorial approach to computational continuum mechanics using object-oriented techniques. Comput. Phys. 12 (6), 620–631.

Wilkening, H., Huld, T., 1999. An adaptive 3-D CFD solver for modeling explosions on large industrial environmental scales. Combust. Sci. Technol. 149 (1–6), 361–387.

Xiao, J., Breitung, W., Kuznetsov, M., Zhang, H., Travis, J.R., Redlinger, R., Jordan, T., 2017a. GASFLOW-MPI: A new 3-D parallel all-speed CFD code for turbulent dispersion and combustion simulations: Part I: Models, verification and validation. Int. J. Hydrog. Energy 42 (12), 8346–8368.

Xiao, J., Breitung, W., Kuznetsov, M., Zhang, H., Travis, J.R., Redlinger, R., Jordan, T., 2017b. GASFLOW-MPI: A new 3-D parallel all-speed CFD code for turbulent dispersion and combustion simulations: Part II: First analysis of the hydrogen explosion in Fukushima Daiichi Unit 1. Int. J. Hydrog. Energy 42 (12), 8369–8381.

Yabing, L., Xianghui, L., Peng, C., Deyang, X., 2022. A conservative approach for the fast deflagration analysis in the containment with GASFLOW-MPI. Front. Energy Res. 10.

Yassin, K., Kelm, S., Kampili, M., Reinecke, E.-A., 2023. Validation and verification of containmentFOAM CFD simulations in hydrogen safety. Energies 16 (16).

Yassin, K., Kelm, S., Reinecke, E.-A., 2025. Numerical simulation of dispersion and ventilation of hydrogen clouds in case of leakage inside a large-scale industrial building. Hydrogen 6 (2).

Zivkovic, D., Sattelmayer, T., 2021. Towards efficient and time-accurate simulations of early stages of industrial scale explosions. In: 9th International Conference on Hydrogen Safety. ICHS 9, Health and Safety Executive, Edinburgh, Scotland.

Zivkovic, D., Sattelmayer, T., 2023. Fractal based, scale-adaptive closure model for Darrieus–Landau instability effects on large-scale hydrogen-air flames. Combust. Sci. Technol. 195 (7), 1573–1598.